Journal Name

ARTICLE

A HER2 selective theranostic agent for surgical resection guidance and photodynamic therapy.

Received 00th January 20xx,
Accepted 00th January 20xx

DOI: 10.1039/x0xx00000x

www.rsc.org/

H. Pye[a], M.A. Butt[a,b], H.W. Reinert[a], A. Maruani[c], J.P.M. Nunes[c], J.S. Marklew[d], M. Qurashi[a,e], L. Funnell[a], A. May[a], I. Stamati[d], R. Hamoudi[a], J.R. Baker[c], M.E.B. Smith[c], S. Caddick[c], M.P Deonarain[a,d,e], G. Yahioglu[d,e]*, V. Chudasama[c]* and L.B. Lovat[a,b]*

In many cancers early intervention involves surgical resection of small localised tumour masses. Inadequate resection leads to recurrence whereas overzealous treatment can lead to organ damage. This work describes production of a HER2 targeting antibody Fab fragment dual conjugated to achieve both real time near-infrared fluorescent imaging and photodynamic therapy. The use of fluorescence emission from a NIR-dye could be used to guide resection of tumour bulk, for example during endoscopic diagnosis for oesophago-gastric adenocarcinoma, this would then be followed by activation of the photodynamic therapeutic agent to destroy untreated localised areas of cancer infiltration and tumour infiltrated lymph nodes. This theranostic agent was prepared from the Fab fragment of trastuzumab initially by functional disulfide re-bridging and site-specific click reaction of a NIR-dye. This was followed by further reaction with a novel pre-activated form of the photosensitiser chlorin e6 with the exposed fragments' lysine residues. Specific binding of the theranostic agent was observed *in vitro* with a HER2 positive cell line and cellular near-infrared fluorescence was observed with flow cytometry. Specific photo-activity of the conjugates when exposed to laser light was observed with HER2 positive but not HER2 negative cell lines *in vitro*, this selectivity was not seen with the unconjugated drug. This theranostic agent demonstrates that two different photo-active functions can be coupled to the same antibody fragment with little interference to their independent activities.

Introduction

The Human Epidermal Growth Factor Receptor 2 (HER2) has no known ligand but can form heterodimers with other members of the family to initiate downstream signalling in cellular pathways that include proliferation, differentiation, angiogenesis and cell survival[1]. Attention was originally drawn to HER2 when it was shown that amplification at both the gene and protein level occur in about 20% of patients with breast cancer and correlated with poor prognosis[2]. HER2 is now implicated in many other cancers including bladder, pancreatic, lung, ovarian, endometrial, colorectal, renal, head and neck, gastric, oesophageal, and prostate cancers[3].

Overexpression of HER2 has been described in gastrointestinal (GI) cancers and was recently validated by our group as positive in 26% of upper oesophago-gastric adenocarcinoma (OGA) patients[4–6]. However, HER2 expression in OGA is heterogeneous and the link between overexpression and patient prognosis remains controversial due to study bias for cancer position or grade alongside subjective scoring and lack of technique standardisation across the field[7–11]. Imaging for this disease is minimally invasive and is performed using an endoscope. Similarly, abdominal surgery is increasingly being performed using laparoscopy. This represents an unique opportunity for the delivery and activation of light activated diagnostic tools and drugs. An estimated 8,000 new cases of oesophageal adenocarcinoma (OA) are diagnosed yearly in the UK with a 5-year survival of 15%. Tumours that present early can be treated by endoscopic resection however, despite high quality imaging tools, small tumours are hard to detect and even when intramucosal cancer is present visible lesions are only found in ~60% of cases[6]. Also visible tumours have indistinct edges and inadequate resection leads to recurrence whereas overzealous treatment leads to intractable oesophageal strictures. Better identification is needed to ensure appropriate treatment both endoscopically and during

[a] *Department for Tissue & Energy, Division of Surgery & Interventional Science, University College London, Cruciform Building, Gower Street, London, WC1E 6AE*
[b] *Upper Gastrointestinal Service, University College London Hospitals NHS Foundation Trust, 250 Euston Road, London, NW1 2PG.*
[c] *Department of Chemistry, University College London 20 Gordon Street, London, WC1H 0AJ*
[d] *Antikor BioPharma, Stevenage Bioscience Catalyst, Gunnels Wood Road, Stevenage, Herts, SG1 2FX.*
[e] *Department of Chemistry, Imperial College London, Exhibition Road, London SW7 2AZ.*
# These authors contributed equally to this work.
* Corresponding authors: l.lovat@ucl.ac.uk (Laurence B Lovat), v.chudasama@ucl.ac.uk (Vijay Chudasama), g.yahioglu@antikor.co.uk (Gokhan Yahioglu).
Electronic Supplementary Information (ESI) available: [Contains more detail on the production of high purity trastuzumab Fab Alkyne, Trastuzumab IgG and trastuzumab. Analysis showing Fab-Alkyne binding positively to other relevant human gastrointestinal tract adenocarcinomas. The methods for the chemical synthesis of the bridging agent (N-propargyl-3,4-dibromomaleimide) and the anhydride-Ce6 and the chemical structure and fluorescence spectra of the two dyes in their free forms; NIR dye and Ce6]. See DOI: 10.1039/x0xx00000x

surgery for larger lesions. Fluorescence imaging is a powerful approach already used in the clinical setting, as is PDT and both are compatible with endoscopy. Therefore a combined approach with more focused targeting and the potential for a 'see-and-treat' modality would be very attractive and potentially straight-forward to implement into clinical practice for OA treatment.

HER2 already provides a validated basis for targeted therapeutics and trastuzumab (Herceptin™) is a humanised monoclonal immunoglobulin G (IgG) against HER2 which alone, and in combination therapy, has been used to successfully treat breast cancer[12,13]. The potential for trastuzumab therapy in GI cancers was shown in the ToGA (Trastuzumab for GAstric Cancer) clinical study[14] leading to its approval for use with chemotherapy for patients with HER2-positive metastatic OGA. The mechanism of resistance to trastuzumab in breast cancer is complex and related to signalling defects rather than receptor down-regulation[15]. This makes an antibody–drug conjugate (ADC) approach attractive for the delivery of cytotoxins directly to the tumour. The most successful ADC to date is trastuzumab emtansine (Kadcyla™,), for treating HER2-positive metastatic breast cancer[16].

Generally, whole antibody formats, such as IgG are retained at high levels in human tumours over longer time periods (days–weeks), but with a lower degree of specificity, their slow penetration means that it takes days for significant levels to accumulate in tumours whilst the Fc-domain leads to significant cross-reaction with normal tissues, especially the liver[17]. Smaller fragments, *e.g.* Fab and scFv are taken up by the tumour more rapidly (within hours as elegantly demonstrated by Denis *et al.*[18]) but at comparatively lower levels and with quicker serum and tumour clearance times[19,20]. This leads to a higher tumour:normal tissue ratio (specificity) which is important for both a therapeutic agent (side-effects) and an imaging agent (contrast)[21].

The use of site-selective antibody conjugation is known to generate well-characterised, homogeneous and reproducible antibody conjugates that behave predictably *in vivo*[22]. Next-generation maleimides and pyridazinediones are intrinsically more stable than conventional maleimide conjugates which can suffer from oxidative loss of payload. Furthermore, the technology can be manipulated to create thiol-stable, acid cleavable or thiol cleavable linkers, as well as target exposed cysteine residues or disulfide bonds as sites for conjugation[23–31]. Previous relevant application of the technology include bi-functional antibody bioconjugation and photosensitiser conjugation to trastuzumab[32–34].

Photodynamic therapy (PDT) is an approved treatment modality for cancer. This approach involves administration of photosensitisers (PS) which accumulate passively in the tumour and are locally activated using laser light. Subsequent cellular destruction occurs *via* reactive oxygen species (ROS) and/or free radicals[35–37]. This approach is a treatment for localised light accessible solid tumours without the toxicity and collateral damage associated with radiotherapy or major surgery. PDT can also activate an immune response to cancer, a key step in establishing a prolonged remission[38–41]. However, a limitation of PDT is its poor tumour selectivity and a suboptimal pharmacokinetic / biodistribution profile. This leads to low potency and prolonged skin photosensitivity which can lead to severe 'sunburn' as well as the development of scarring and structuring of internal organs including the oesophagus[42]. This has hindered the acceptance of this powerful treatment as a standard cancer treatment modality. Antibody-based photodynamic therapy, in particular with antibody fragments, aims to overcome these problems by reducing non-specific uptake of PS and improve PS clearance rates[43–46]. We have previously demonstrated that HER2-expressing tumours can be eradicated *in vivo* using an scFv conjugated to the PS pyropheophorbide-a, but this PS did not have a useful imaging read-out making it unattractive as a potential theranostic[44]. Further development of this as a PDT agent only and not a theranostic will be published elsewhere.

The targeting vehicle for our theranostic approach herein is based on a trastuzumab Fab fragment. Fab molecules still maintain all the pharmacokinetic benefits of smaller antibody fragments but can cope with higher drug loading due to their slightly larger size, the presence of a disulphide bond also lends itself better than an ScFv to the application of two different conjugation techniques. The Fab was prepared to a high quality from the parent molecule using sequential enzyme digest. An endogenous disulphide was replaced using an alkyne-bearing next-generation maleimide. This alkyne allowed the efficient conjugation of an azide-containing NIR-dye (IR Dye 800 CW) to the Fab through highly specific 'click' chemistry resulting in an exceptionally pure product with one bright NIR-dye molecule covalently attached to each Fab molecule. This commercial NIR dye was chosen due to its high quality, the fact it is manufactured under cGMP and because it is already undergoing multiple clinical trials in an ADC form[47]. Chlorin e6 was chosen as the PS because it is a well studied PS with high water solubility and high singlet oxygen yield[48]. Its initial conjugation to the functionalised Fab fragment was attempted through classical acyl urea chemistry involving activation of one of the carboxylic acid residues using *N*-hydroxysuccinimide and a carbodiimide dehydrating agent, but with limited success due to the multifunctional nature of chlorin e6. A cleaner and more efficient conjugation was achieved using a pre-activated anhydride form of chlorin e6 which reacts with surface lysine residues through selective ring opening resulting in amide bond formation but without the crosslinking seen with the *in situ* carbodiimide conjugation approach. The PS and NIR dye components were specifically chosen so that the absorbance spectrum of the PS was as far into the red as possible to allow deeper light penetration and an optical spectrum that was not interfered by the excitation and imaging of the NIR dye. The chemistries for the conjugation were chosen to be bi-orthogonal and compatible for commercial application. The resulting theranostic antibody fragment (Fab-NIR-PS) was shown to be applicable to NIR fluorescence cell-labelling of HER2 positive oesophageal adenocarcinoma cells *in vitro.* It was also tested in an *in vitro* model of PDT in which it exhibited improved PDT cytotoxicity and HER2-expressing cell specificity compared to the equivalent unconjugated PDT drug.

Results and Discussion

Production of trastuzumab Fab alkyne

To produce high purity trastuzumab Fab alkyne, high quality trastuzumab IgG (Roche) underwent sequential enzymatic digest; the most common glycoform of trastuzumab IgG is 148059 Da[49]. LC-MS demonstrated that the pepsin digested trastuzumab-F(ab')$_2$, had an observed mass of 97303 Da. The trastuzumab-F(ab')$_2$ fragment was further digested with papain to obtain the Fab fragment with an observed mass of 47635 Da by Agilent LC-MS. The interchain disulfide was reduced using TCEP and the purified fragment was analysed by Agilent LC-MS with observed masses of 24200 Da and 23439 Da to reveal the heavy and light chains only, thus confirming that fully reduced trastuzumab Fab had been produced. The reduced trastuzumab Fab was then re-bridged using a bridging agent (*N*-propargyl-3,4-dibromomaleimide) that permits site-specific and stoichiometric (1:1) introduction of a single alkyne functional group onto the Fab fragment with a yield of 96%[50]. Non-reducing SDS-PAGE and Agilent LC-MS analysis (Fig. 1) confirmed the protein was pure and of the expected molecular weight with an LC-MS observed mass of 47785 Da compared to the expected mass of 47786 Da. (More detail in Supplementary data).

Selective binding of trastuzumab Fab-alkyne to HER2 positive cells

To investigate the ability of the modified antibody to bind to cells *in vitro,* trastuzumab Fab-alkyne was analysed by flow cytometry with two different cell lines. OE19 is a HER2 positive human epithelial cell line established from a stage three moderately differentiated OGA, and was recently validated against the original pathology sample[51,52]. U-87 (U-87 MG) is a human glial cell line established from a grade IV glioblastoma of the brain[53] and was used as a negative control for HER2 expression. A FITC conjugated secondary antibody was used to detect any trastuzumab bound to cells (Fig. 2). With OE19 cells both the trastuzumab IgG and the trastuzumab Fab-alkyne showed a dose-dependant increase in the fluorescence signal. Saturation of the fluorescence signal indicated cell surface expression. A FITC conjugated secondary antibody was used to detect any trastuzumab bound to cells (Fig. 2). With OE19 cells both the trastuzumab IgG and the trastuzumab Fab-alkyne showed a dose-dependant increase in the fluorescence signal. Saturation of the fluorescence signal indicated cell surface receptor saturation. With the Fab-alkyne very little binding affinity was lost compared to the native IgG despite the loss of the avidity effect. (NB no change in binding affinity was seen between Fab and Fab-alkyne). Nonlinear regression analysis using standard 2-parameter, 1:1 binding equations allowed an estimation of the dissociation constant K_d for these antibodies on this cell line which were as follows; trastuzumab IgG K_d = 11.8nM, trastuzumab Fab-alkyne K_d = 43.7 nM. There was no non-specific cell binding of either antibody format to the HER2 negative line. Trastuzumab IgG and trastuzumab Fab-alkyne also bound specifically to other HER2 positive human gastrointestinal tract adenocarcinomas including, OE33 an oesophageal cancer line and NCI-N87 a gastric cancer line (Supplementary data).Using the functional re-bridging of a native interchain disulfide bond, a non-native reactive chemical alkyne group was introduced away from the antibody binding site which preserved the structural integrity of the molecule while providing a stable covalently bound alkyne group at 1:1 stoichiometry in 100% of the molecules reacted.

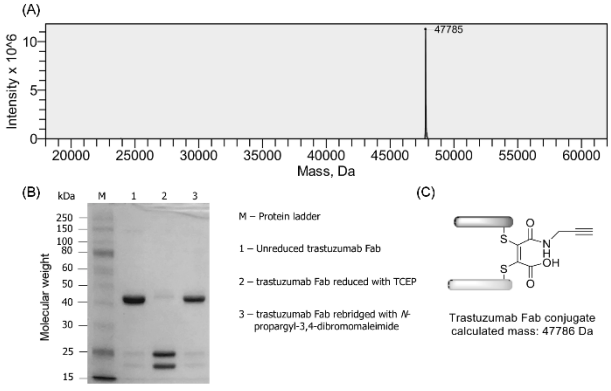

Fig 1.Characterisation of trastuzumab Fab-alkyne on (A) an Agilent system LC-MS and shows a pure product of the predicted molecular weight; data deconvoluted. (B) Non-reducing SDS-PAGE data stained with Coomassie. Picture insert (C) shows the chemical detail of the modified disulphide bridging within the antibody fragment

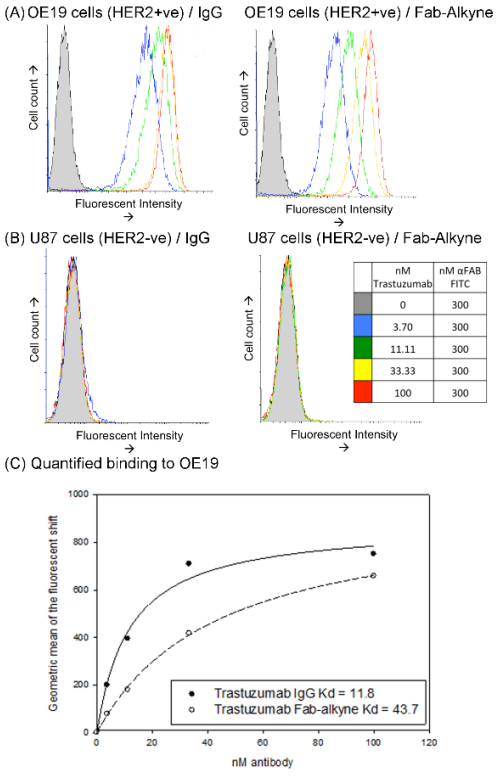

Fig 2. Binding of trastuzumab Fab-alkyne compared to its parent molecule trastuzumab IgG onto a HER2 positive oesophageal adenocarcinoma cell line (OE19) using flow cytometry (A). An increase in fluorescence represents more trastuzumab has bound to each cell and the saturation of the fluorescent signal indicates cell surface receptor saturation. Very little binding affinity is lost in the Fab despite the loss of bi-valency. Neither version bound the human glioblastoma cell line U87 (control for HER2 negativity) (B). Binding to the HER2 positive line was quantified using the geometric means of the fluorescent shift curves. This is shown in (C) with nonlinear regression analysis fitted to a 1:1 binding isotherm to calculate the dissociation constant Kd; Equation fitted as follows (f = Bmax*abs(x)/(Kd + abs(x)). Trastuzumab IgG Kd = 11.8 nM, trastuzumab Fab-alkyne Kd = 43.7 nM.

Formation of the Fab-NIR dye conjugate

To add the imaging agent a near-infrared (NIR) dye, IR Dye 800 CW (LiCOR), carrying an azide functional group was linked on the alkyne functionalised Fab fragment using bio-compatible click chemistry[54]: (supplementary data). A small proportion of protein was lost upon purification resulting in a yield of ~85%. Samples of the 'Fab-NIR' imaging agent were taken throughout the purification process for analyses and quality control on SDS-PAGE (Fig. 3a, 3b). These showed that unconjugated NIR dye was successfully removed from the final product by desalting. In the post-conjugation samples NIR dye fluorescence was seen co-localised with the protein band at ~48 kDa demonstrating the conjugation is covalent. The conjugated Fab migrated at a slightly higher MW compared to the Fab alone due to the addition of the dye.

To calculate the efficiency of the 'click' reaction a diluted sample of Fab-NIR was analysed by UV-Vis spectroscopy (Fig. 3c). Extinction coefficients of the free dye and protein were used to determine the dye and protein concentrations of the conjugate. The protein absorption at 280nm was corrected for NIRdye and it was assumed that absorbance at 776 nm was from the NIR dye alone. There were no significant shifts in spectra between the free and conjugated dye (Fig. 3c). Protein concentrations for multiple reactions were also determined by Bradford assay. The reaction was reproducible, and despite manipulation of experimental parameters, UV-Vis spectroscopy showed the NIR dye drug-to-antibody ratio ((NIR)DAR) never exceeded 0.7. LC-MS was carried out on a Thermo-Scientific system, and the NIR-conjugated Fab was compared to the unconjugated Fab-alkyne, results demonstrated that the reaction had reached completion with a (NIR)DAR of 1. The LC-MS showed a single product peak with an observed mass of 48951 Da, within accepted limits when compared to the expected mass of 48954 Da (Fig. 4). It is likely that dye interactions with the protein surface are adversely affecting the dye extinction coefficient, leading to an under-estimation by UV-Vis spectroscopy.

A pure and characterised NIR fluorescent trastuzumab fab molecule was produced with a stable covalently bound NIR dye at 1:1 stoichiometry. The addition of the NIR dye to our theranostic complies with modern homogenous antibody drug conjugate production methods.

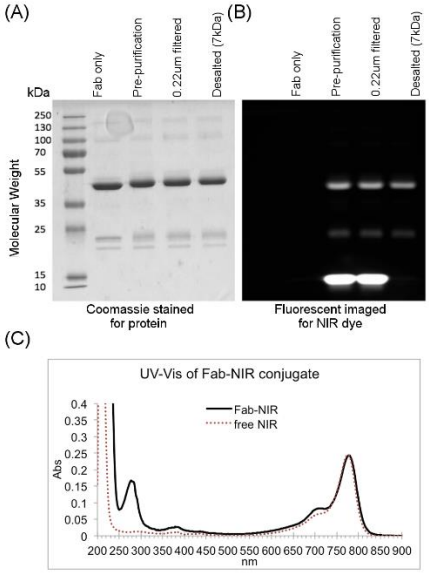

Fig 3. Characterisation of the imaging agent; Fab-NIR. Samples of the NIR dye-Fab taken throughout the conjugation and purification process and ran on non-reducing SDS-PAGE; Gels were Coomassie stained for protein (A) after imaging for NIR fluorescence (B). Unconjugated dye (seen at the dye front with the 10 kDa marker) was removed from the final product and any dye remaining was covalently bound. Fab-NIR was analysed by UV-Vis spectroscopy (C) shown overlayed with the spectrum of free NIR dye (dotted red) to show lack of shifts in spectra between the free and conjugated dye.

Formation of the Fab-NIR-PS theranostic conjugate

Conjugation of photosensitisers to antibodies and antibody fragments is technically challenging; it has been previously shown that PS insolubility can (negatively) affect conjugate pharmacokinetics, conjugation efficiency and hinder purification of non-covalently bound free PS after conjugation[44,46,55]. In order to demonstrate a clear proof-of-concept, a well-characterised and studied PS called chlorin e6 (Ce6) was selected. Chlorin e6 has a high singlet oxygen quantum yield and a strong absorption at around ~660 nm, away from the absorption peak of the NIR dye ~780nm, together with relatively high water solubility[48].

Conjugation of chlorin e6 to the Fab-NIR fragment was initially attempted using *in situ* carbodiimide (EDC) / *N*-hydroxysuccinimide (NHS) mediated chemistry between the carboxyl groups on the Ce6 and primary amine lysine residues on the antibody. However, cross-linking was a major side-reaction reducing both the purity and yield of the final conjugate as well as significantly reducing binding of the antibody to the antigen. Cross-linking was most likely caused by either excess EDC coupling agent or by the over-activation of more than one carboxylic acid group on the Ce6 molecule. Our data suggested that it was over activated Ce6 which was

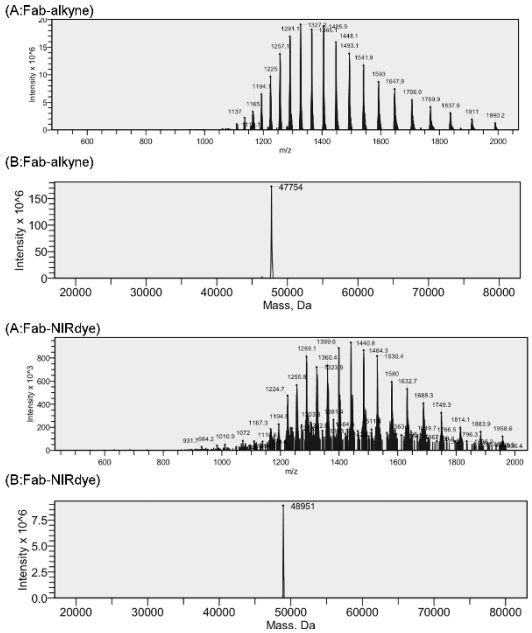

Fig 4. LC-MS characterisation of trastuzumab Fab-alkyne pre conjugation and trastuzumab Fab-NIR post conjugation on a Thermo Scientific system LC-MS shows a NIR dye conjugated product. The expected mass increase of 1197 Da between the samples matches the mass of the NIR-Dye without counter-ions (1200 Da). LC-MS data non-deconvoluted (A) and deconvoluted (B).

responsible for the cross linking, therefore, reduced reaction times and excess NHS led to a reduction in protein cross-linking, although not to an acceptable level.

To overcome protein cross-linking during the *in situ* procedure, we developed a method for chlorin e6 conjugation *via* the pre-formation of an anhydride ring between two carboxylic acid groups on the Ce6 molecule. This means reactions can be carried out without the need for a carbodiimide crosslinker and reduces the three reactive groups on Ce6 to one so cross-linking reactions should not be able to occur. This molecule was described previously as a temporarily formed molecular intermediate in the synthesis of talaporfin but has not to our knowledge ever been used in bio-conjugation[56]. Chlorin e6 anhydride was prepared through a modified and improved procedure (supplementary data) and reaction with exposed epsilon-amines on the lysine side chains of the Fab fragment should result in ring opening and covalent amide bond formation. A similar reaction has been reported for a DOTA-anhydride with trastuzumab[57].

Samples of the purified theranostic antibody–drug conjugate 'Fab-NIR-PS' were analysed by SDS-PAGE. Photosensitisers are inherently fluorescent so the gel was imaged for NIR dye and PS fluorescence before fixing and staining (Fig. 5a–c). Almost all unconjugated PS was removed by desalting. A proportion of highly conjugated and aggregated antibody in which NIR fluorescence was quenched was also removed during the purification process.

To determine NIRdye, PS and protein concentrations within the conjugate, a diluted sample of the Fab-NIR-PS was analysed by UV-Vis spectroscopy using correction factors calculated from the free dyes and applied to any wavelengths where more than one molecule absorbed (Fig. 5d). Protein concentrations were also determined by Bradford assay. Based on these measurements, an average PS drug-to-antibody ratio ((PS)DAR) of 4.4 was obtained as an average over four independent batches (standard deviation between batches below 1), protein yield was always above 70%. When the material lost during purification was analysed by SDS-PAGE it was shown to contain insoluble Fab monomers with a higher conjugation ratio rather than cross-linked protein.

Compared to the free dyes, the absorbance spectrum of the Fab-NIR-PS conjugates show peak broadening at ~400 nm and red-shifts at ~660 nm and ~780 nm suggesting the extinction coefficients are influenced by the protein environment. Conjugates were also diluted into final 6 M urea solutions and analysed by UV-Vis spectroscopy to see if unfolding the protein would resolve any shifts and allow more accurate UV-Vis spectroscopic analysis but no effect on the spectrum was observed.

Spectroscopic analyses seemed to show that the (NIR)DAR dropped to 0.45 in the theranostic (Fab-NIR-PS) compared to 0.7 in the dye alone conjugate (Fab-NIR). The absorption spectrum also showed red-shift in NIR dye peak absorption. This suggested that the extinction coefficient for the NIR dye had changed upon Ce6 conjugation rather than NIR dye has been released from the Fab-NIR dye conjugate. This is supported by the absence of free NIR dye on SDS-PAGE for the un-purified double conjugate (Fig. 4). It was not possible to analyse the Fab-NIR-PS with the current method of LC-MS due to complications caused by the mixture of species generated but it would be possible with a modified technique[58].

Conjugation to accessible lysine residues produces a heterogeneous product distribution around an average loading

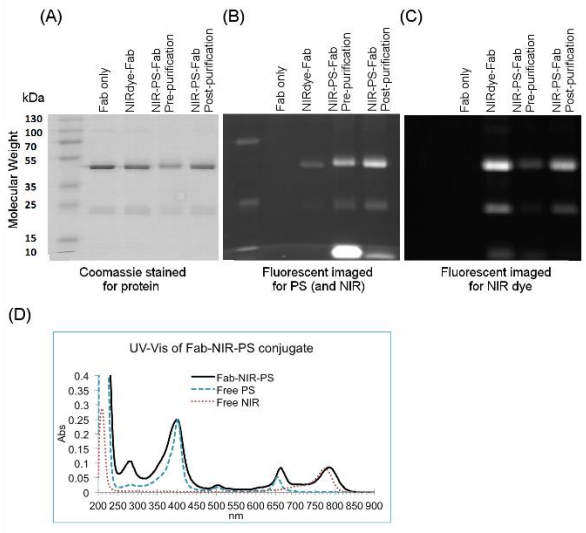

Fig 5. Characterisation of the theranostic agent; trastuzumab Fab-NIR-PS. Samples of the Fab-NIR-PS were taken throughout the conjugation and purification process run on non-reducing SDS-PAGE; gels were Coomassie stained for protein (A) after being imaged for PS fluorescence (B) and NIR fluorescence (C). Almost all unconjugated dye (seen at the dye front with the 10 kDa marker) was removed from the final product and the dye was covalently bound. Fab-NIR-PS was analysed by UV-Vis spectroscopy (D) shown overlayed with a spectrum of free PS (dashed blue) and free NIR dye (dotted red). The Ce6 peak at 402 nm only broadened upon conjugation but the 660 nm Ce6 peak red shifted (663 nm conjugate vs 654 nm free) and the NIR dye peak at 780 nm also red-shifted (787 nm conjugate vs 778nm free).

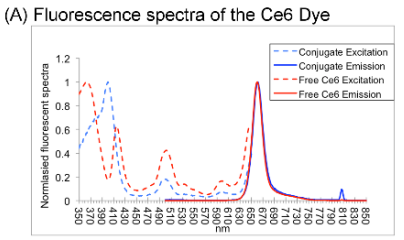

Wavelength of main peak			Excitation at 402nm of matched absorbance	
Chlorin e6	Excitation	Emission	Counts per second	%
Free Dye	361	660	2991310	100
Conjugate	400	661	238270	8

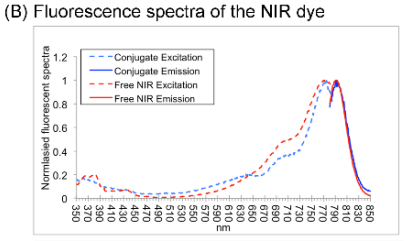

Wavelength of main peak			Excitation at 776nm of matched absorbance	
NIR Dye	Excitation	Emission	Counts per second	%
Free Dye	771	793	38918	100
Conjugate	773	791	7490	19

Fig 6. Fluorescent spectra of the double conjugate compared to free dye. Samples of Fab-NIR-PS, free NIR dye and free Ce6 were matched for their absorbance peaks. Fluorescent spectra were read for (A) the Ce6 dye (Ex 402 nm Em 660 nm) and (B) the NIR dye (Ex 776 nm Em 792 nm). Presented spectra were normalised to the maximal counts per second (CPS) in each sample. Fluorescent peaks were observed as shown and showed no significant shifts in emission spectra from either dye apart from around 400 nm for the Ce6. Both dyes can still be excited independently with limited cross-over of energy. Raw fluorescent values for comparable samples show loss of fluorescent efficiency is seen after conjugation for both the Ce6 (8% of free dye) and NIR dye (19% of free dye).

ratio. This average loading ratio can be changed by manipulation of the reaction conditions. When the reaction between Ce6-anhydride and Fab-NIR was optimised products of higher conjugation ratios (average (PS)DAR > 5) were either insoluble in aqueous solution at pH 7.4 or showed significantly reduced antigen binding. The addition of excipients failed to maintain solubility or was detrimental to purification. The reaction was therefore optimised for the highest loading efficiencies that could maintain their solubility in PBS pH 7.4 at 4 °C. Further evaluation of excipients or the introduction of another solubilising chemical group on the hydrophobic side of the Ce6 tetrapyrrole ring may improve payload loading and solubility or higher (PS)DARs may be possible using antibody fragment frameworks optimised for high payload loading[44].

Using a pre-activated Ce6 molecule a theranostic antibody–ADC was synthesised with an average therapeutic (PS)DAR of 4. A product with the same specifications could be produced reliably and reproducibly between independent experiments. Although state-of-the-art conjugation techniques focus on homogeneous ADC production, all ADCs currently marketed and in late phase clinical trials are mixed product conjugates[59]. When conditions are controlled a predictable and quantifiable composition can be produced which can be accurately analysed by mass spectrometry techniques; examples of this in clinically relevant conjugates can be found from Immunogen and Genetech, these conjugates translate into predictable and well characterised pharmacokinetic data[58,60–63]. Trastuzumab emtansine has between 0 and 7 loaded drugs (average DAR of 4) this ADC is IgG based, the range of products produced with our Fab is predicted to be lower.

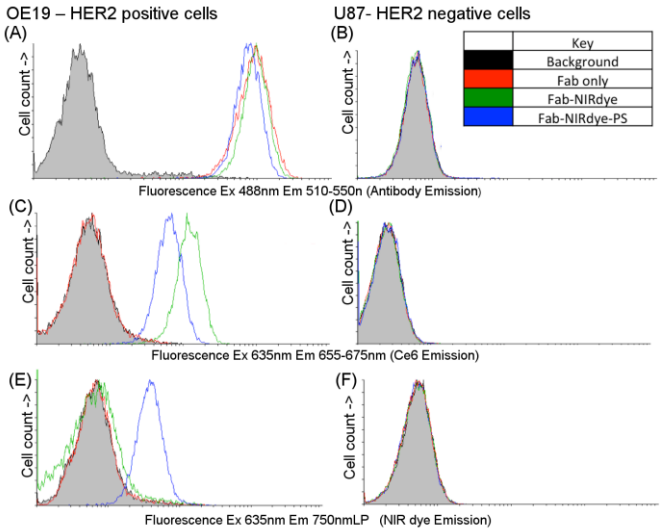

Fig 7. *In vitro* cell binding of trastuzumab Fab-NIR dye and trastuzumab Fab-NIR dye-PS. Binding was tested on the cell line OE19, a human oesophageal adenocarcinoma with high HER2 expression (A,C,E) and U87, a human glioblastoma cell line and control for HER2 negativity (B,D,F). Cell staining was carried out on ice with a sub cell surface saturation concentration of the primary antibody trastuzumab in one of three forms; un-conjugated (red), conjugated to NIR dye only (green) and conjugated to both NIR and PS (blue). This was followed by an excess of anti-Fab antibody conjugated to a FITC fluorophore so antibody binding could be directly measured by an increase in FITC fluorescence (A,B), cells were also measured for fluorescence from the NIR dye (C,D) and for fluorescence from the PS dye (E,F).

Fluorescence characterisation of the theranostic agent

In order to confirm that the two components could be activated independently, the fluorescence excitation and emission profiles of the Fab-NIR-PS were analysed (Fig. 6). There were no shifts in emission spectra from either conjugated dye when compared to free dye and both dyes could be excited independently. Transfer of energy was limited to a small amount from Ce6 to NIR dye, seen by a shift in the shoulder of the NIR excitation peak at ~660 nm and a fluorescence emission peak at ~790 nm when Ce6 was excited at 402nm. When absorbance spectra were matched at wavelengths for Ce6 and NIR excitation and the fluorescence output measured, loss of fluorescence efficiency was seen after conjugation for both the Ce6 (8% of free dye) and NIR dye (19% of free dye).

HER2 specific NIR cellular imaging of the theranostic agent

To establish if the NIR dye was sufficiently fluorescent for cell labelling and if there was any loss of antibody binding upon single payload NIR dye conjugation or double payload NIR-PS conjugation, flow cytometry was carried out to measure binding to HER2 positive OE19 cells (Fig. 7). Detection of the Fab molecule was carried out under sub cell surface saturation conditions previously validated to be on the linear region of the binding curve for this experimental setup. Any changes in binding efficiency are seen as shifts in fluorescent signal; no shifts were seen with the Fab-NIR compared to Fab only, a slight but insignificant shift in antibody binding was seen with the Fab-NIR-PS suggesting PS are only slightly interfering with antigen-epitope recognition**.** Any effect on kinetic binding constants could be quantified using isolated antigen and surface plasmon resonance (*i.e.* Biacore™). Labelled cells could easily be detected through both NIR-dye and PS emission. Single colour controls were used to ensure there was no bleed-through between the three detection wavelength ranges once compensated appropriately. The reduction in NIR fluorescence between the single and double conjugate, despite equivalent cell binding, supports the argument that the NIR dye is quenched slightly by the Ce6 in the double conjugate. Cells negative for HER2 expression showed no binding of either conjugate.

HER2 targeted PDT cytotoxicity of the theranostic agent

To investigate the potential use of the conjugate for targeted PDT, HER2 positive and negative cells were incubated at 37 °C for 1 hour in the dark with either the theranostic agent (Fab-NIR-PS) or equivalent amounts of free Ce6 before exposure to a final dose of 5 J/cm^2 of 670 nm light over 60 seconds (Fig. 8 and Fig. 9). A much lower total light dose than used clinically (100–200 J/cm^2) was applied because as light travels into any tissue it quickly loses energy due to the scattering and absorbing properties of the tissue. For this reason sub-picomolar cytotoxicities obtainable by high light dose are not relevant for *in vivo* translation. Instead presented here is the limit of lowest effective toxicity with low light dose.. Control samples showed no cytotoxicity of the drug without laser irradiation or from laser irradiation alone (Fig 8.).

Upon laser irradiation the theranostic agent exhibited dose dependent cytotoxicity for HER2 positive cells with an IC_{50} of 1.8μM (Fig 8.). If the IC_{50} of Fab-NR-PS is calculated as concentration of Ce6 within the conjugate, *i.e.* the the 4:1 ratio of photosensitizer conjugation is taken into account the IC_{50} of the conjugate is 7.3 uM per3uM Ce6. Free unconjugated Ce6 has an IC_{50} of 15.5uM with the same cell line (Fig9.) There was no observable cytotoxicity of Fab-NR-PS with the HER2 negative cell line U87 whereas cytoxicity with the free unconjugated Ce6 in this line was IC_{50} = .9.1uM. The relative large error bars are to be expected due to small variations of light dose across the beam area, despite this when analysed with area under the curve analysis according to Cleves *et al.*[64], the Fab-NIR-PS induced cytotoxicity was significantly (p=0.04) higher for HER2 positive cells than the HER2 negative cells (Fig 9.). When the same analysis was carried out with the data with the free unconjugated PS there was no significant difference in cytotoxicity between the two cell lines (Fig 9.).

Typically, targeted PDT agents demonstrate potencies in the high nanomolar to micromolar range, this is lower than other published ADCs due to the lower cytotoxicity of singlet oxygen compared to the highly potent payloads used in current ADCs, however, other PDT ADCs have led to significant tumour reduction *in vivo*, and have shown multiple dosing is well tolerated alongside a favourable side-effect profile [44,45,65].

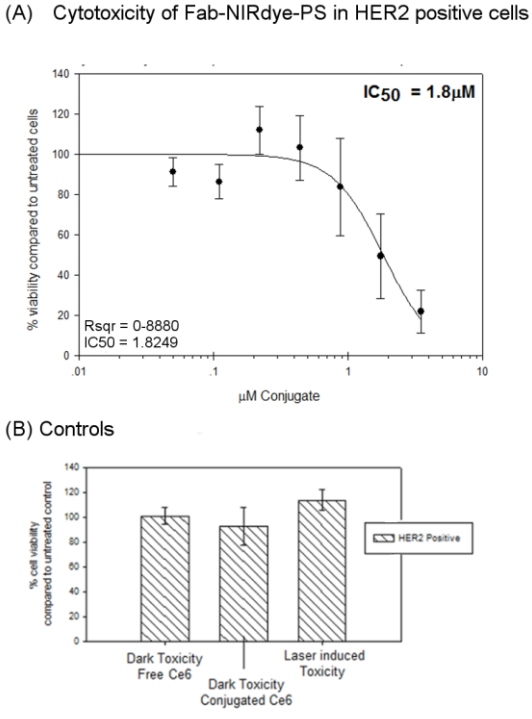

Fig 8. Dose dependent PDT based cytotoxicity of the Fab-NIR-PS in a HER2 positive cell line (A) controls are shown in (B). All experiments undergo the same PDT treatment; cells were exposed to various concentrations of the drug over one hour at 37 °C, cells are then washed twice prior to exposing cells to a 670 nm laser at 5 J/cm^2. Cell viability was measured 24 hours later via MTT assay. The IC_{50} of Fab-NIR-PS at this light does in this cell line was 1.8 μM. Controls show no toxicity of Fab-NIR-PS or equivalent free Ce6 without light or toxicity from the laser alone.

Based on our own experience the cytotoxicity is within a range that can affect *in vivo* tumour growth if the PK, vasculature and immune parameters also important for effective PDT are in place. Based on this we would expect our Fab-NIR-PS to have anti-tumour activity in preclinical models.

Conclusions

Conjugation of two different optically-active moieties, a near-infrared imaging dye at 790 nm and a 670 nm laser activated photodynamic therapy drug to a trastuzumab Fab was shown to produce an effective and promising theranostic antibody–drug conjugate. The theranostic agent retained binding and was selective for its target *in vitro* as demonstrated by NIR imaging and antigen-specific cytotoxicity. With further development, we believe this theranostic agent shows potential as an adjunctive therapy for HER2 positive OGA.

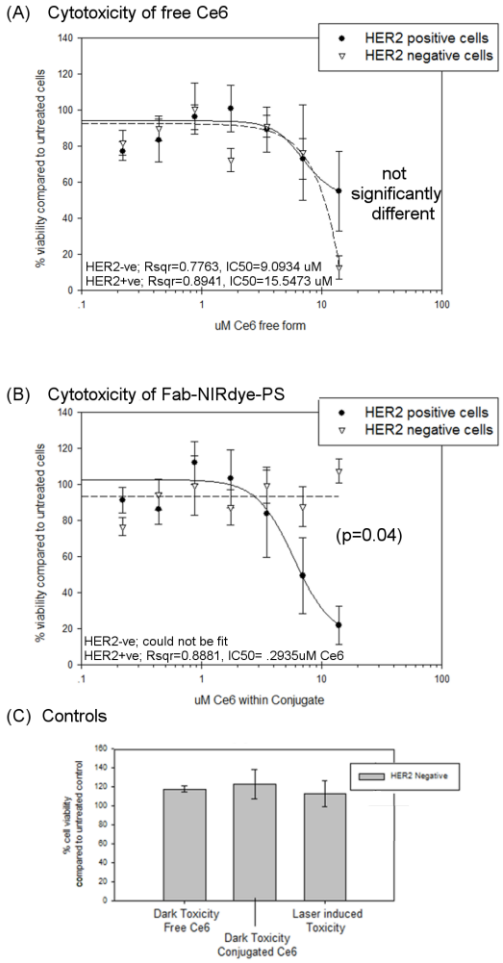

Fig 9. Dose dependent PDT based cytotoxicity of Fab-NIR-PS (B) compared to free PS (A) in HER2 positive and HER2 negative cell lines. Controls for the HER2 negative line are shown in (C). Data is presented as 'concentration of Ce6 within the theranostic drug' so it can be better compared with free drug. All experiments undergo the same PDT treatment; cells were exposed to various concentrations of the drug over one hour at 37 °C, cells are then washed twice prior to exposing cells to a 670 nm laser at 5 J/cm^2. Cell viability was measured 24 hours later via MTT assay. Fab-NIR-PS was shown to be significantly more cytotoxic for HER2 positive cells than HER2 negative cells (p=0.04), with the free PS there was no significant difference in cytotoxicity between HER2 positive cells than HER2 negative cells.

Experimental

LC-MS: was performed on protein samples using either an *Agilent system* or a *Thermo Scientific system*; both consisted of a uPLC column: Hypersil Gold C4 1.9 µm, 2.1µm × 50 µm connected to MSQ Plus Single Quad Detector (SQD) with the following parameters. *Agilent system;* Wavelength: 254 nm. Mobile Phase: 95:5 Water:MeCN (0.1% formic acid) to 5:95 Water:MeCN (0.1% formic acid) gradient over 7-20 min. Flow Rate: 0.4 mL/min. MS Mode: ES+. Scan Range: m/z = 500–2400. Scan time: 1.0 s. Data obtained in continuum mode. The electrospray source of the MS was operated with a capillary voltage of 3.5 kV and a cone voltage of 35 V. Nitrogen was used as the nebulizer and desolvation gas at a total flow of 650 L/h. Ion series were generated by integration of the total ion chromatogram (TIC) over the 2.8–3.3 or 4–5 min range. Total mass spectra for protein samples were reconstructed from the ion series using MassLynx V4.0 SP4 software. *Thermo Scientific system;* Wavelength: 254 nm. Mobile Phase: 99:1 Water (0.1% formic acid): MeCN (0.1% formic acid) to 1:9 Water (0.1% formic acid): MeCN (0.1% formic acid) gradient over 4 min. Flow Rate: 0.3 mL/min. MS Mode: ES+. Scan Range: *m/z* = 100 – 2000. Scan time: 1.5 s. Data obtained in continuum mode. The electrospray source of the MS was operated with a capillary voltage of 3.5 kV and a cone voltage of 50V. Nitrogen was used as the nebulizer and desolvation gas at a total flow of 600 L/h. Total mass spectra for protein samples were reconstructed from the ion series using the pre-installed ProMass software using default settings for large proteins in *m/z* range 500–2000.

SDS-PAGE: Samples diluted into pH6.8 Tris-HCl loading buffer with final concentration of 2% SDS and 10% glycerol without reducing agents or tracking dyes and boiled for 5 minutes at 70-100 ˚C. Gels were hand cast 1 mm gels with a discontinuous buffer system containing 0.1% APS and 0.1% TEMED to polymerise; *Resolving gel:* 12% acrylamide/bis 0.1% SDS, in 0.37 M Tris-HCl pH8.8. *Stacking gel:* 4% acrylamide/bis 0.1% SDS, in 0.12 M Tris-HCl pH6.8. Samples were loaded at 2 µg protein alongside a marker (Thermo 26619). Gels ran at 30 mA per gel until bands well resolved in 1X running buffer (0.25M Trisma base + 2.5 M glycine + 0.1% SDS). Un-stained gels were imaged for fluorescence using a CCD camera flat bed imager (G:BOX CHEMI HR1.4, Syngene) and long pass filters (Horiba); NIR dye (Ex 720–763 nm, Em780LP), Photosensitiser (Ex 450–485 Em:650LP). Gels were then fixed and stained with 0.1% Coomassie Brilliant Blue G in a 10% acetic acid 40% methanol buffer.

UV-Vis spectroscopy; Read using a Lambda 25 (Perkin Elmer) in a micro volume 1cm path length quartz cuvette, samples diluted 1:20 into PBS (pH7.4). Spectra normalised to 900 nm and solvent background removed. Concentrations were calculated using the following equation A = εlc where A is absorbance of the sample, ε = molar absorptivity, l = path length in cm and c = concentration in molar. Molar extinction coefficient (M^{-1} cm^{-1}) were calculated in PBS pH 7.4 as follows; trastuzumab FAB-alkyne 280 nm ε = 68590, NIR dye 280 nm ε = 5827, 402 nm ε = 0, 776 nm ε = 188179, Ce6-anhydride 280 nm ε = 9816, 402 nm ε = 81020. Molecular weights (Da) calculated as follows; trastuzumab FAB-alkyne = 47786, NIR dye = 1269 and Ce6-anhydride = 579.

Bradford Assay: Samples were diluted 1:25 into Bradford reagent (Sigma B6916) in a 96 well plate, shaken (350 rpm) for 5-10 minutes at room temperature then measured at 630 nm on a ELx800 Absorbance Microplate reader (BioTek). A standard curve of BSA was included on each plate and read simultaneously. BSA and trastuzumab Fab were shown to create identical standard curves and samples were loaded at a concentration below which NIR or PS dye would contribute to absorbance at 630 nm within the assay, previously calculated.

Production of reduced trastuzumab Fab: To prepare trastuzumab-F(ab')$_2$ immobilized pepsin (0.6 mL) was washed with digestion buffer (20 mM sodium acetate trihydrate, pH 3.1) four times and trastuzumab (Roche) (2 mL, 6.47 mg/mL in digestion buffer) was added. The mixture was incubated for 5 h at 37 ºC whilst shaking (1100 rpm). Resin was separated from the digest using a filter column, and washed with digest buffer (50 mM phosphate, 1 mM EDTA, 150 mM NaCl, pH 6.8) three times. The digest was combined with the washes and the volume adjusted to 2 mL. Immobilized papain (2 mL, 0.25 mg/mL) was activated with 10 mM DTT (in digest buffer: 50 mM phosphate, 1 mM EDTA, 150 mM NaCl, pH 6.8) whilst shaking (1100 rpm) for 1 h at 37 °C. Resin was washed with digest buffer (without DTT) four times and the 2 mL of trastuzumab-F(ab')$_2$ added. The mixture was incubated for 48 h at 37 °C whilst shaking (1100 rpm). Then, resin was separated from the digest using a filter column, and washed with BBS (25 mM sodium borate, 25 mM NaCl, 1 mM EDTA, pH 8.0) three times. The digest was combined with the washes and the buffer was exchanged completely for BBS using diafiltration columns (GE Healthcare, 10 kDa MWCO) and the volume adjusted to 2 mL. To affect reduction of the interchain disulfide TCEP (240 µL, 6.5 mM) was added to a solution of Fab fragment (8 mL, 65 µM, 3.1 mg/mL in 25 mM sodium borate, 25 mM NaCl, 1 mM EDTA, pH 8.0) and incubated for 1.5 h at 37 °C.

Production of trastuzumab Fab Alkyne: For chemical synthesis of *N*-propargyl-3,4-dibromomaleimide see the supplementary data or as published[50]. To effect re-bridging of the interchain disulphide *N*-propargyl-3,4-dibromomaleimide (50 µL per mL of reduced trastuzumab Fab, 6.5 mM solution in DMF) was added to a solution of reduced trastuzumab Fab fragment (65 µM, 3.1 mg/mL in 25 mM sodium borate, 25 mM NaCl, 1 mM EDTA, pH 8.0). After 1 h at 20 °C, the excess *N*-propargyl-3,4-dibromomaleimide was removed by repeated ultrafiltration (GE Healthcare, 10 kDa MWCO) into fresh buffer (PBS, pH 7.4).

Production of trastuzumab Fab NIR imaging agent (Click chemistry): Trastuzumab Fab-alkyne was 0.22 µm spin filtered, then desalted (7 kDa MWCO Zeba) into 0.22 µm filtered PBS pH 7.4. For a 500 µL reaction volume; trastuzumab Fab-alkyne was diluted to a final concentration of 65 µM in PBS (pH 7.4) containing final concentrations of tris(3-hydroxypropyltriazolylmethyl)amine (THPTA) (605 µM), $CuSO_4$ (121 µM) and aminoguanidine·HCl (5 mM). The THPTA and $CuSO_4$ (stocks in deionised water stored at 4 °C) were premixed with each other at a 5:1 ratio just before use, aminoguanidine·HCl made up fresh in deionised water just

before use. To this mixture the azide containing molecule (Licor IR Dye 800CW Azide Infrared Dye Cat;929-60000) was added at 12 equivalents to the alkyne (final concentration 800 µM) and final DMSO at 5% (v/v). Dye stock in anhydrous DMSO stored in the dark at -20 ˚C. Sodium ascorbate added last to the mixture (final concentration 4.5 mM, made up fresh in deionised water just before use). Reaction mixture incubated in a closed eppendorf in the dark on a flat bed shaker (125 rpm) at 37 °C overnight (~20 h). The sample was then subjected to centrifugal force to remove any precipitated material (10,000 g, 2 minutes) and filtered through a 0.22 µm filter. Excess reagents were removed by desalting (7 kDa MWCO Zeba) into fresh buffer (PBS, pH 7.4).

Production of trastuzumab Fab NIR-Ce6 theranostic agent (Anhydride chemistry): For chemical synthesis of chlorin e6-anhydride (Ce6-Anhydride) see supplementary data. Ce6-anhydride (Antikor Biopharma) was stored as a solid at 4 °C in the dark under vacuum in a desiccator. The anhydride is hydrolysed over time in aqueous solution to its open ring form. Inactivated Ce6 (Medkoo Biosciences Cat. 500410) was stored in the dark at -20 ˚C. Handling of the photosensitive drugs and subsequent conjugates was whereever possible carried out under dim light conditions. At least 24 hours prior to reaction the Ce6-anhydride was made up at 20 mg/mL in anhydrous DMSO, snap frozen and stored at -20 °C. The drug could be used reliably in this form up to a week after it was frozen. For a 700 µL reaction volume; trastuzumab Fab-NIR dye was diluted to a final concentration of 20 µM in PBS (pH 7.4). To this the Ce6-anhydride was added at 20 equivalents to the protein (final concentration 400 µM) and final DMSO at 20%. Reaction mixture incubated in a closed eppendorf in the dark on a flat bed shaker (125 rpm) at 37 °C for 2 hours. The sample was then subjected to centrifugal force to remove any precipitated material (10,000 g, 2 minutes) and filtered through a 0.22 um filter. Excess reagents were removed by desalting (7kDa MWCO Zeba) into fresh buffer (PBS, pH 7.4).

Fluorescent spectral analysis: Samples were diluted in PBS pH 7.4 into a small volume quartz cuvette to ensure peak absorbance was below 0.25 absorbance units and absorption for the excitation wavelength was matched between free and conjugated dye within 0.05 absorbance units (Agilent 8453 spectrophotometer). The cuvette was transferred to the spectrofluorometer (Horiba Jobin Yvon Fluoromax-4) and maintained at 20–22 °C. The emission spectra were corrected at each wavelength for the sensitivity of the detector and the excitation spectra were corrected at each wavelength for the lamp intensity (FluorEssence) and the second harmonic. Spectra were normalised to the maximal counts per second (CPS) in each sample. Where samples are presented together or compared all read settings were identical including excitation wavelength, em/ex slits and integration time of the signal.

***In vitro* cell culture;** OE19 cells were obtained from the ECACC May 2014 and U87-MG were a kind gift from Dr M. P. Deonarain, Imperial College London, 2010. All lines were cultured according to ECACC guidelines. Cells were confirmed mycoplasma free and kept within a 20 passage range.

Flow cytometry: Cells were detached with Accutase, and 200,000 cells per sample were washed and incubated in 50 µL on ice with various concentrations of trastuzumab. After 1 hour cells were washed and exposed to 300 nM α-Human IgG (Fab specific) FITC conjugate (SIGMA F5512) on ice for 30 minutes before two final washes. All steps carried out in FC buffer; PBS + 2% FCS + 1 mM EDTA. Flow cytometry was carried out on a Beckman-Coulter Cyan ADP, FITC detection channel; (Ex 488 nm Em 510–550 nm), NIR dye detection channel; (Ex 635 nm Em750LP), PS detection channel; (Ex 635 nm Em655–675). Data was taken from the fluorescent signal of 10,000 cells gated to exclude, doublets, aggregates and debris. Data was analysed and quantified using the geometric mean of the curve using Flowing Software Version 2.5.1 (Perttu Terho, Turku Centre for Biotechnology, Finland). For analysis of the ADCs trastuzumab antibodies were incubated at 50 nM because this was shown to be just under cell surface saturation of OE19 cells (Fig. 2).

Photodynamic therapy (PDT): Cells were plated in clear bottomed black walled 96 well plates at 25,000 cells (OE19) or 12,000 cells (U87) per well, plates for U87 cells were pre-coated with attachment factor (cell systems 4Z0-210). Cell number was previously calibrated to ensure endpoint signal was not saturated and cells were not over-confluent. The following day media was replaced with 100 µL media containing experimental compound at varying concentrations. Plates were protected from light and incubated at 37 °C and 5% CO_2 for one hour, cells were washed twice with PBS and returned to 200 µL media before being exposed to a 670 nm Laser (Hamamatsu LD670C) at a dose of 5 J/cm^2 over 60 seconds at 80 mW/cm^2. Cells not irradiated were protected by a cardboard shield, plates were protected from light and returned to the incubator. Light was delivered *via* fibre optic / frontal light distributor (model FD-1 Medlight S.A SN FD1-1345) and calibrated for exact energy delivery (Gentec TDM-300 / PSV-3103). 24 h later, media was replaced with 200 µL MTT reagent (Sigma-Aldrich M5655) at 0.5 mg/mL in FCS free cell culture media. (MTT is a tetrazolium salt based assay and measures cell viability by the detection of cellular reducing equivalents such as NADH that are produced during normal cellular metabolism.) Plates were protected from light and incubated at 37 °C and 5% CO_2 for three hours, MTT media was then replaced by 100 µL DMSO and shaken (350 rpm) for 10–15 minutes until all crystals had dissolved before the absorbance at 490 nm was measured on a ELx800 Absorbance Microplate reader (BioTek). For IC_{50} Equation fitted using sigma plot; four Parameter Logistic Curves with equation; f1 = min + (max-min)/(1 + (x/EC50)^(-Hillslope)), constrained min=0, max=100.

Acknowledgements

Funding for this project was from Innovate UK (formerly the Technology Strategy Board) (grant reference 131439) and Antikor Biopharma (formerly PhotoBiotics Ltd). Flow cytometry data was analysed and quantified using freeware created by Perttu Terho, (Turku Centre for Biotechnology, Finland). The laser and light delivery systems were on loan from Antikor BioPharma and calibrated using equipment from Sandy Mosse

(University College London). The flow cytometry facility was provided by Tomas Adejumo as part of the Wolfson Institute (University College London) and the LC-MS facilities were provided by Kersti Karu (Agilent) or the Caddick group (Thermo Scientific) both part of the Department of Chemistry (University College London). Fluorescent spectroscopy was carried out courtesy of Marina Kuimova (Imperial College London). The lab of Lovat LB is supported by the CRUK UCL Early Cancer Medicine Centre and the Department of Health's National Institute for Health Research Biomedical Research Centres funding scheme. The views expressed in this publication are those of the authors and not necessarily those of the Department of Health. The authors associated with the Dept. of Chemistry at UCL also gratefully acknowledge the EPSRC, BBSRC, BRC, Wellcome Trust, HEFCE, SBC, MRC, UCL and UCLB for support of their programme. We also thank Dr. Hayley Whitaker for critically reading our manuscript.

Notes and references

1 N. E. Hynes and H. A. Lane, *Nat. Rev. Cancer*, 2005, **5**, 341–54.

2 D. J. Slamon, W. Godolphin, L. A. Jones, J. A. Holt, S. G. Wong, D. E. Keith, W. J. Levin, S. G. Stuart, J. Udove and A. Ullrich, *Science*, 1989, **244**, 707–12.

3 S. Ménard, P. Casalini, M. Campiglio, S. Pupa, R. Agresti and E. Tagliabue, *Ann. Oncol.*, 2001, **12 Suppl 1**, S15–9.

4 S. F. Schoppmann, B. Jesch, J. Friedrich, F. Wrba, A. Schultheis, U. Pluschnig, J. Maresch, J. Zacherl, M. Hejna and P. Birner, *Am. J. Surg. Pathol.*, 2010, **34**, 1868–73.

5 C. Gravalos and A. Jimeno, *Ann. Oncol.*, 2008, **19**, 1523–9.

6 M. A. Butt, M. Gandy, R. J. Haidry, E. S. Bloom, S. Mackie, M. S. Khan, J. Louis-Auguste, D. Oukrif, S.-U.-R. Khan, R. Saraswati, M. R. Banks, M. Rodriguez-Justo, L. B. Lovat and M. Novelli, *Gut*, 2013, **62**, A112–A113.

7 T. C. Chua and N. D. Merrett, *Int. J. Cancer*, 2012, **130**, 2845–56.

8 H. H. Yoon, Q. Shi, W. R. Sukov, A. E. Wiktor, M. Khan, C. A. Sattler, A. Grothey, T.-T. Wu, R. B. Diasio, R. B. Jenkins and F. A. Sinicrope, *Clin. Cancer Res.*, 2012, **18**, 546–54.

9 Y. Y. Janjigian, D. Werner, C. Pauligk, K. Steinmetz, D. P. Kelsen, E. Jäger, H.-M. Altmannsberger, E. Robinson, L. J. Tafe, L. H. Tang, M. A. Shah and S.-E. Al-Batran, *Ann. Oncol.*, 2012, **23**, 2656–62.

10 H. H. Yoon, Q. Shi, W. R. Sukov, M. A. Lewis, C. A. Sattler, A. E. Wiktor, T.-T. Wu, R. B. Diasio, R. B. Jenkins and F. A. Sinicrope, *J. Clin. Oncol.*, 2012, **30**, 3932–8.

11 P. Stahl, C. Seeschaaf, P. Lebok, A. Kutup, M. Bockhorn, J. R. Izbicki, C. Bokemeyer, R. Simon, G. Sauter and A. H. Marx, *BMC Gastroenterol.*, 2015, **15**, 7.

12 C. L. Arteaga, M. X. Sliwkowski, C. K. Osborne, E. A. Perez, F. Puglisi and L. Gianni, *Nat. Rev. Clin. Oncol.*, 2012, **9**, 16–32.

13 Y. Yarden and G. Pines, *Nat. Rev. Cancer*, 2012, **12**, 553–63.

14 Y.-J. Bang, E. Van Cutsem, A. Feyereislova, H. C. Chung, L. Shen, A. Sawaki, F. Lordick, A. Ohtsu, Y. Omuro, T. Satoh, G. Aprile, E. Kulikov, J. Hill, M. Lehle, J. Rüschoff and Y.-K. Kang, *Lancet (London, England)*, 2010, **376**, 687–97.

15 T. A. Bailey, H. Luan, R. J. Clubb, M. Naramura, V. Band, S. M. Raja and H. Band, *J. Carcinog.*, 2011, **10**, 28.

16 I. E. Krop, S.-B. Kim, A. González-Martín, P. M. LoRusso, J.-M. Ferrero, M. Smitt, R. Yu, A. C. F. Leung and H. Wildiers, *Lancet. Oncol.*, 2014, **15**, 689–99.

17 D. Litvak-Greenfeld and I. Benhar, *Adv. Drug Deliv. Rev.*, 2012, **64**, 1782–99.

18 M. S. Dennis, H. Jin, D. Dugger, R. Yang, L. McFarland, A. Ogasawara, S. Williams, M. J. Cole, S. Ross and R. Schwall, *Cancer Res.*, 2007, **67**, 254–61.

19 V. Kenanova and A. M. Wu, *Expert Opin. Drug Deliv.*, 2006, **3**, 53–70.

20 S. M. Deyev and E. N. Lebedenko, *Bioessays*, 2008, **30**, 904–18.

21 M. P. Deonarain, G. Yahioglu, I. Stamati and J. Marklew, *Expert Opin. Drug Discov.*, 2015, **10**, 463–481.

22 P. Agarwal and C. R. Bertozzi, *Bioconjug. Chem.*, 2015, **26**, 176–92.

23 C. R. Behrens, E. H. Ha, L. L. Chinn, S. Bowers, G. Probst, M. Fitch-Bruhns, J. Monteon, A. Valdiosera, A. Bermudez, S. Liao-Chan, T. Wong, J. Melnick, J.-W. Theunissen, M. R. Flory, D. Houser, K. Venstrom, Z. Levashova, P. Sauer, T.-S. Migone, E. H. van der Horst, R. L. Halcomb and D. Y. Jackson, *Mol. Pharm.*, 2015.

24 A. Maruani, S. Alom, P. Canavelli, M. T. W. Lee, R. E. Morgan, V. Chudasama and S. Caddick, *Chem. Commun. (Camb).*, 2015, **51**, 5279–82.

25 M. T. W. Lee, A. Maruani, J. Baker, S. Caddick and V. Chudasama, *Chem. Sci.*, 2016, **7**, 799–802.

26 V. Chudasama, M. E. B. Smith, F. F. Schumacher, D. Papaioannou, G. Waksman, J. R. Baker and S. Caddick, *Chem. Commun. (Camb).*, 2011, **47**, 8781–3.

27 M. E. B. Smith, M. B. Caspersen, E. Robinson, M. Morais, A. Maruani, J. P. M. Nunes, K. Nicholls, M. J. Saxton, S. Caddick, J. R. Baker and V. Chudasama, *Org. Biomol. Chem.*, 2015, **13**, 7946–9.

28 P. Moody, M. E. B. Smith, C. P. Ryan, V. Chudasama, J. R. Baker, J. Molloy and S. Caddick, *Chembiochem*, 2012, **13**, 39–41.

29 C. P. Ryan, M. E. B. Smith, F. F. Schumacher, D. Grohmann, D. Papaioannou, G. Waksman, F. Werner, J. R. Baker and S. Caddick, *Chem. Commun. (Camb).*, 2011, **47**, 5452–4.

30 L. Castañeda, A. Maruani, F. F. Schumacher, E. Miranda, V. Chudasama, K. A. Chester, J. R. Baker, M. E. B. Smith and S. Caddick, *Chem. Commun. (Camb).*, 2013, **49**, 8187–9.

31 J. P. M. Nunes, M. Morais, V. Vassileva, E. Robinson, V. S. Rajkumar, M. E. B. Smith, R. B. Pedley, S. Caddick, J. R. Baker and V. Chudasama, *Chem. Commun. (Camb).*, 2015, **51**, 10624–7.

32 F. Bryden, A. Maruani, H. Savoie, V. Chudasama, M. E. B. Smith, S. Caddick and R. W. Boyle, *Bioconjug. Chem.*, 2014, **25**, 611–7.

33 A. Maruani, M. E. B. Smith, E. Miranda, K. A. Chester, V. Chudasama and S. Caddick, *Nat. Commun.*, 2015, **6**, 6645.

34 A. Maruani, H. Savoie, F. Bryden, S. Caddick, R. Boyle and V. Chudasama, *Chem. Commun. (Camb).*, 2015, **51**, 15304–

7.
35 A. P. Castano, T. N. Demidova and M. R. Hamblin, *Photodiagnosis Photodyn. Ther.*, 2005, **2**, 1–23.
36 A. P. Castano, T. N. Demidova and M. R. Hamblin, *Photodiagnosis Photodyn. Ther.*, 2005, **2**, 91–106.
37 A. P. Castano, T. N. Demidova and M. R. Hamblin, *Photodiagnosis Photodyn. Ther.*, 2004, **1**, 279–93.
38 C. Bastianpillai, N. Petrides, T. Shah, S. Guillaumier, H. U. Ahmed and M. Arya, *Tumour Biol.*, 2015, **36**, 9137–46.
39 E. Reginato, P. Wolf and M. R. Hamblin, *World J. Immunol.*, 2014, **4**, 1–11.
40 M. Korbelik, *Photochem. Photobiol. Sci.*, 2011, **10**, 664–9.
41 A. P. Castano, P. Mroz and M. R. Hamblin, *Nat. Rev. Cancer*, 2006, **6**, 535–45.
42 B. F. Overholt, K. K. Wang, J. S. Burdick, C. J. Lightdale, M. Kimmey, H. R. Nava, M. V Sivak, N. Nishioka, H. Barr, N. Marcon, M. Pedrosa, M. P. Bronner, M. Grace and M. Depot, *Gastrointest. Endosc.*, 2007, **66**, 460–8.
43 M. Mitsunaga, M. Ogawa, N. Kosaka, L. T. Rosenblum, P. L. Choyke and H. Kobayashi, *Nat. Med.*, 2011, **17**, 1685–1691.
44 M. Bhatti, G. Yahioglu, L. R. Milgrom, M. Garcia-Maya, K. A. Chester and M. P. Deonarain, *Int. J. Cancer*, 2008, **122**, 1155–63.
45 A. Palumbo, F. Hauler, P. Dziunycz, K. Schwager, A. Soltermann, F. Pretto, C. Alonso, G. F. Hofbauer, R. W. Boyle and D. Neri, *Br. J. Cancer*, 2011, **104**, 1106–15.
46 H. Pye, I. Stamati, G. Yahioglu, M. Butt and M. Deonarain, *Antibodies*, 2013, **2**, 270–305.
47 LI-COR; Registered Clinical Trials with probes labeled with IRDye® 800CW, *https://www.licor.com/clinical_translation/registered_clinical_trials.html*, Accessed 03 2016.
48 R. W. Redmond and J. N. Gamlin, *Photochem. Photobiol.*, 1999, **70**, 391–475.
49 C. W. N. Damen, W. Chen, A. B. Chakraborty, M. van Oosterhout, J. R. Mazzeo, J. C. Gebler, J. H. M. Schellens, H. Rosing and J. H. Beijnen, *J. Am. Soc. Mass Spectrom.*, 2009, **20**, 2021–33.
50 L. Castañeda, Z. V. F. Wright, C. Marculescu, T. M. Tran, V. Chudasama, A. Maruani, E. A. Hull, J. P. M. Nunes, R. J. Fitzmaurice, M. E. B. Smith, L. H. Jones, S. Caddick and J. R. Baker, *Tetrahedron Lett.*, 2013, **54**, 3493–3495.
51 J. C. Rockett, K. Larkin, S. J. Darnton, A. G. Morris and H. R. Matthews, *Br. J. Cancer*, 1997, **75**, 258–63.
52 J. J. Boonstra, R. van Marion, D. G. Beer, L. Lin, P. Chaves, C. Ribeiro, A. D. Pereira, L. Roque, S. J. Darnton, N. K. Altorki, D. S. Schrump, D. S. Klimstra, L. H. Tang, J. R. Eshleman, H. Alvarez, Y. Shimada, H. van Dekken, H. W. Tilanus and W. N. M. Dinjens, *J. Natl. Cancer Inst.*, 2010, **102**, 271–4.
53 J. Pontén and E. H. Macintyre, *Acta Pathol. Microbiol. Scand.*, 1968, **74**, 465–86.
54 V. Hong, S. I. Presolski, C. Ma and M. G. Finn, *Angew. Chem. Int. Ed. Engl.*, 2009, **48**, 9879–83.
55 M. K. Kuimova, M. Bhatti, M. Deonarain, G. Yahioglu, J. A. Levitt, I. Stamati, K. Suhling and D. Phillips, *Photochem. Photobiol. Sci.*, 2007, **6**, 933–9.
56 J. A. Hargus, F. R. Fronczek, M. G. H. Vicente and K. M. Smith, *Photochem. Photobiol.*, **83**, 1006–15.
57 M. Moreau, O. Raguin, J.-M. Vrigneaud, B. Collin, C. Bernhard, X. Tizon, F. Boschetti, O. Duchamp, F. Brunotte and F. Denat, *Bioconjug. Chem.*, 2012, **23**, 1181–8.
58 A. Wakankar, Y. Chen, Y. Gokarn and F. S. Jacobson, *MAbs*, **3**, 161–72.
59 P. Sapra and B. Shor, *Pharmacol. Ther.*, 2013, **138**, 452–69.
60 L. Wang, G. Amphlett, W. A. Blättler, J. M. Lambert and W. Zhang, *Protein Sci.*, 2005, **14**, 2436–46.
61 A. C. Lazar, L. Wang, W. A. Blättler, G. Amphlett, J. M. Lambert and W. Zhang, *Rapid Commun. Mass Spectrom.*, 2005, **19**, 1806–14.
62 J. Marcoux, T. Champion, O. Colas, E. Wagner-Rousset, N. Corvaïa, A. Van Dorsselaer, A. Beck and S. Cianférani, *Protein Sci.*, 2015, **24**, 1210–23.
63 S. Girish, M. Gupta, B. Wang, D. Lu, I. E. Krop, C. L. Vogel, H. A. Burris Iii, P. M. LoRusso, J.-H. Yi, O. Saad, B. Tong, Y.-W. Chu, S. Holden and A. Joshi, *Cancer Chemother. Pharmacol.*, 2012, **69**, 1229–40.
64 M. A. Cleves, *Stata J.*, 2002, **2**, 301–313.
65 M. D. Savellano, N. Owusu-Brackett, J. Son, T. Ganga, N. L. Leung and D. H. Savellano, *Photochem. Photobiol.*, **89**, 687–97.